

The radiative effect of an aged, internally mixed Arctic aerosol originating from lower-latitude biomass burning

By ANN-CHRISTINE ENGVALL^{1*}, JOHAN STRÖM², PETER TUNVED³, RADOVAN KREJCI³, HANS SCHLAGER⁴ and ANDREAS MINIKIN⁴, ¹Norwegian Institute for Air Research (NILU), P.O. Box 100, N-2027 Kjeller, Norway; ²Norwegian Polar Institute, 9296 Tromsø, Norway; ³Department of Applied Environmental Science – Atmospheric Science Unit, Stockholm University, 106 91, Stockholm, Sweden; ⁴Deutsches Zentrum für Luft- und Raumfahrt (DLR), Institut für Physik der Atmosphäre, Oberpfaffenhofen, 82234 Weßling, Germany

(Manuscript received 21 May 2008; in final form 28 May 2009)

ABSTRACT

Arctic-haze layers and their radiative effects have been investigated previously in numerous studies as they are known to have an impact on the regional climate. In this study, we report on an event of an elevated aerosol layer, notably consisting of high-absorbing soot particles, observed in the European Arctic free troposphere the 2007 April 14 during the ASTAR 2007 campaign. The ca. 0.5 km vertically thick aerosol layer located at an altitude of around 3 km had a particle-size distribution mode around 250 nm diameter. In this study, we quantify the radiative effect aerosol layers have on the Arctic atmosphere by using in situ observations. Measurements of particles size segregated temperature stability using thermal denuders, indicate that the aerosol in the optically active size range was chemically internally mixed. In the plume, maximum observed absorption and scattering coefficients were 3×10^{-6} and $20 \times 10^{-6} \text{ m}^{-1}$, respectively. Observed microphysical and optical properties were used to constrain calculations of heating rates of an internally mixed aerosol assuming two different surface albedos that represent snow/ice covered and open ocean. The average profile resulted in a heating rate in the layer of 0.2 K d^{-1} for the high-albedo case and 0.15 K d^{-1} for the low albedo case. This calculated dependence on albedo based on actual observations corroborates previous numerical simulations. The heating within the plume resulted in a measurable signal shown as an enhancement in the temperature of a few tenths of a degree. Although the origin of the aerosol plume could not unambiguously be determined, the microphysical properties of the aerosol had strong similarities with previously reported biomass burning plumes. With a changing climate, short-lived pollutants such as biomass plumes may become more frequent in the Arctic and have important radiative effects at regional scale.

1. Introduction

Forest fires are known to emit large amounts of trace gases and aerosols, which can be subsequently transported over large distances and influence the atmospheric chemistry and radiation balance far from the source region (e.g. Forster et al., 2001; Fiebig et al., 2003). Black carbon (BC), sometimes referred to as soot, is an important light-absorbing aerosol component arising from the burning of biomass and fossil fuel. Soot aerosols in the atmosphere absorb incoming solar radiation as well as the

backscattered radiation from the Earth's surface, which gives rise to a heating of the atmosphere (Lohmann and Feichter, 2005; Seinfeld, 2008).

Not only elevated concentrations of light-absorbing aerosol, but also its mixing state plays an important role for the radiative properties. Jacobson (2001) has shown that the internal mixing of soot has a larger effect on global warming than that caused by external mixing, and may nearly balance the net cooling from other anthropogenic aerosol constituents. Furthermore, Jacobson suggested that the warming due to soot might be the second most important component of global warming after CO_2 in terms of direct forcing.

Penner et al. (1998) estimate the radiative forcing associated with emissions of carbonaceous aerosol from combustion of fossil fuel of ranges from $+0.16$ to $+0.20 \text{ W m}^{-2}$, depending on the soot fraction of the carbon. The direct forcing due to

*Corresponding author.

e-mail: ace@nilu.no

DOI: 10.1111/j.1600-0889.2009.00431.x

carbonaceous aerosol from biomass burning was estimated to be in the range from -0.23 to -0.16 W m^{-2} .

The Arctic is a pristine region, which is very sensitive to external perturbations. A recent climate assessment shows a warming trend in the Arctic that is a factor of two larger than the global average (IPCC, 2007). Light-absorbing aerosol deposited on snow and ice in the Arctic has a significant effect of the radiation budget since it lowers albedo (Hansen and Nazarenko, 2004).

The heating effect of the absorbing aerosol in the atmosphere is known to be larger in the presence of clouds and/or a highly reflecting surface (Lavoué et al., 2000), and thus long-range transports of pollution resulting from biomass burning into the Arctic from lower latitudes are of special importance (Stohl et al., 2006).

The Arctic Study of Tropospheric Aerosols, Clouds and Radiation (ASTAR) 2007 campaign took place in Svalbard between 2007 March 26 and April 17. The period was chosen to collect and investigate data during the period of the year when the Arctic atmosphere is characterized by Arctic haze, that is, long-range transport from the more polluted areas at lower latitudes. Arctic-haze layers and their radiative effects have been investigated previously in numerous studies (e.g. Rinke et al., 2004; Treffeisen et al., 2004, 2007). During the campaign 2007, an event with an elevated layer at an altitude of about 3 km and characterized by high concentrations of light absorbing particles was observed. These types of layers are random in space and time and hence difficult to target in dedicated airborne experiment such as ASTAR. Hence, singular events like this require case studies rather than statistical ensembles.

Due to recent discussions (e.g. IPCC, 2007) about the Arctic temperature amplification, these plumes are of special interest as short-lived pollutants such as methane, ozone and aerosols are estimated to have a combined warming potential of the same magnitude as the long-lived greenhouse gases (Quinn et al., 2008). In this study we contribute to the body of observations that characterize these plumes in order to move towards better model parametrizations in the future of their radiative effects. We calculate the atmospheric heating rate based on the observed vertical size distribution, the absorption and scattering coefficients, as well as information about the state of mixing based on a volatility differential mobility analyser (DMA) system. Information about the aerosol mixing state in the Arctic region from aircraft measurements is still not very common. For anthropogenic pollutants there are obvious mitigation opportunities with respect to the warming of the Arctic by reducing the emissions of light absorbing particles and short-lived greenhouse gases. A change in anthropogenic emissions would bring about a quick response in the climate forcing. However, emissions from forest fires will not be so easy to control, and with a changing climate there is a possibility that timing and frequency of natural fires may change as well.

In this study, we estimate quantitatively the radiation effect of an elevated aerosol layer in the Arctic by using in situ observations in a one-dimensional radiation model. Below we present a description of the experimental methods and the radiation model, followed by observations, summary and discussion.

2. Experimental methods

In this study, we have analysed in situ observations of aerosol number densities of particles larger than 10 and 260 nm in diameter (henceforth denoted N_{10} and N_{260} , respectively), aerosol size distributions, aerosol light scattering and absorption, aerosol mixing state and concentrations of carbon monoxide (CO) and ozone (O_3).

The measurements were performed from the German DLR Falcon 20 research aeroplane. The sample air was brought to the instrumentation via a backward-facing 1/4 inch stainless-steel inlet. The sampling efficiency for a similar inlet on the same aeroplane was investigated by Schröder and Ström (1997) and inlet cut-off was determined to be around 800 nm.

N_{10} was measured using a condensation particle counter (CPC) model TSI 3010. The aerosol size distribution between 17 and 239 nm was measured with a Differential Mobility Particle Sizer (DMPS) in stepwise mode utilizing 13 size-bins (i.e. particle size classes), each of which was measured during 10 s. The size-bins are chosen to fit the inversion program that is used to calculate the size distribution of the aerosol. Thus, the system delivered one size distribution about every other minute. Even though the aerosol number densities are quite low, often only around 100 cm^{-3} , the counting-statistics uncertainties are smaller than 5% (one standard deviation) for the size-distribution mode (increasing towards each end of the distribution).

The aerosol size distribution between 260 and 2200 nm was observed with an optical particle counter (OPC) GRIMM, model 3.709, which sized the particles in 12 bins at 1 Hz. The OPC was connected to a forward-facing near-isokinetic inlet. For a composite aerosol size distribution covering size range from 17 to 2200 nm, OPC data were averaged and merged with the DMPS-derived size distribution.

We also used information about the mixing state of the aerosol in the size range between 17 and 239 nm obtained from a Volatility DMPS (V DMPS). Half of the sample flow downstream of the DMA was directed to a custom-built thermodenuder, where the aerosol was heated to $250 \text{ }^\circ\text{C}$ and the number of particles remaining after heating was counted with the CPC TSI 3010. Due to the difference between saturator and condenser temperatures this CPC had cut-off at 6 nm. A temperature of $250 \text{ }^\circ\text{C}$ was chosen to evaporate volatile and semi-volatile aerosols (e.g. sulphate, bisulphate and a large fraction of organics). Size-dependent losses in the system were determined experimentally prior to the campaign and the data were corrected accordingly.

Information about the light-absorbing properties of the aerosol was obtained from a custom-built particle soot absorption photometer (PSAP), which provided the particle light-absorption coefficient σ_{ap} at a wavelength of 525 nm. From this we estimated the BC mass concentration (ng m^{-3}) by using the commonly employed specific absorption coefficient $10 \text{ m}^2 \text{ g}^{-1}$ (Petzold et al., 1997). The light-scattering properties of the aerosol were measured using an integrating nephelometer (Radiance Research, model M903) at a wavelength of 530 nm.

To characterize the origin of the air masses, information about carbon monoxide (CO) and ozone (O_3) concentrations were used. Details about the instrumentation for measuring these gases can be found in, e.g. Huntrieser et al. (2007).

As a part of the data quality control, an intercomparison was made with measurements from the Zeppelin station (474 m a.s.l.) at Ny-Ålesund (Ström et al., 2003; Engvall et al., 2008). This indicated good agreement between the airborne and the ground-based size-distribution results for particles of diameter smaller than approximately 200 nm. However, the airborne OPC appears to underestimate the number concentration of particles larger than 260 nm by an average factor of around 3.6 compared to the size distribution observed at the Zeppelin station. A correction is made when applying the radiation model, as it is shown in the following section.

3. Radiation model

To investigate the radiative effects of the enhanced aerosol layer a one-dimensional radiation model was used to simulate the amplified heating rate (K d^{-1}). The calculations were based on in situ measurements of the input variables, i.e. relative humidity (RH), temperature (T), pressure (p), aerosol size distribution and the scattering and absorption properties of the aerosols. A brief description of the model is presented here; for more details see Treffeisen et al. (2007).

The aerosol optical properties were estimated using the Mie code MIEV0 (Wiscombe, 1979). This procedure requires an input of the Mie-size parameter and the complex refractive index of the particles to calculate the scattering efficiency, the extinction efficiency and the asymmetry parameter of individual aerosol particles. The optical characteristics of the individual particles were based on the measured properties by assuming internal mixtures (as indicated by measurements) of only soot and sulphate, their relative mass fractions assumed to be equal over the entire size range. The hygroscopic growth of the particles was estimated using standardized growth factors for different compounds from the Global Aerosol Data Set (GADS; Köpke et al., 1997).

The wavelength-dependent refractive index of soot is taken from a parametrization presented by Chang and Charalampopoulos (1990) and the refractive index of sulphate is taken from the GADS data set. The refractive index of internally mixed particles was calculated using the Maxwell–Garnett approxima-

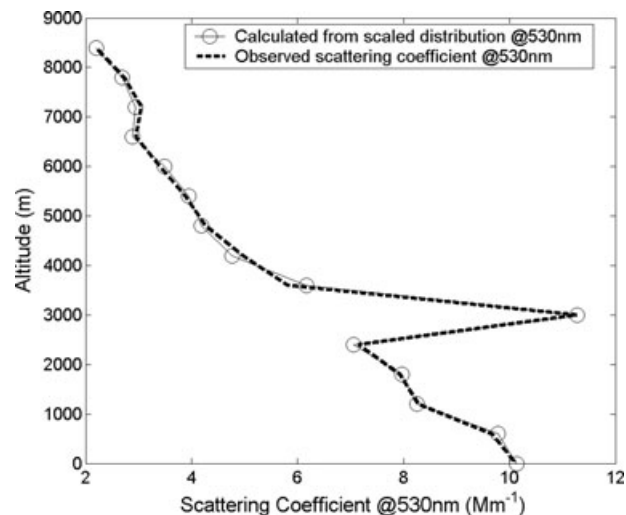


Fig. 1. The observed and the derived scattering profile using the iterative approach described in Treffeisen et al. (2007).

tion, where the densities of soot and sulphate were assumed to be 1000 and 1700 kg m^{-3} , respectively.

The Santa Barbara DISORT Atmospheric Radiative Transfer code (SBDART) is used to calculate the radiative transfer between 0.25 and $4 \mu\text{m}$ (Ricchiuzzi et al., 1998). To capture the polluted layer the vertical model resolution was set to 0.6 km in the lowermost 8.4 km. Furthermore, as the particle-size distributions were measured with a temporal resolution of about 2 min, altitude-intervals of 0.6 km proved to ensure a sufficient number of scans in each model layer. Above 8.4 km altitude a vertical increment of 4 km was used.

In order to test the accuracy of the model-derived optical properties, the 530-nm scattering profile was calculated and compared with its measured counterpart. These results indicated that the Mie-calculations under-predict the measured scattering profile. As previously discussed, the airborne OPC results appear to underestimate the particles by a factor of around 3.6, cf. Fig. 1. Furthermore, since the Zeppelin-station nephelometer results are in agreement with those from the airborne nephelometer, this further confirms that the airborne OPC results should be corrected. Thus the optical scattering estimates used in the model were based on the aircraft-measured size distributions adjusted to the nephelometer data, cf. the procedure used by (Treffeisen et al., 2007) when dealing with the simultaneous LIDAR extinction measurements. These comparisons were undertaken under the assumption of 0% relative humidity, which are the conditions assumed for the observations.

4. Observations

4.1. Aerosol and trace-gas characteristics of the layer

The forthcoming analysis is focused on the mission flight, which took place on 2007 April 14. During the ascent a layer with



Fig. 2. The plume visualized from the aircraft. (Photo by A.-C. Engvall.)

enhanced particle and trace-gas concentrations was detected in the free troposphere. In the course of the return stage of the flight this layer was investigated more closely, cf. Fig. 2.

The layer was located at altitudes between 3000 and 3500 m. Outside the plume (in the free troposphere, FT) the mean (and standard deviation) concentrations of CO and O₃ were estimated to be 156(11) ppb and 57(11) ppb, respectively. The mean and standard deviation of CO and O₃ in the plume do not differ from those in the FT, 164(8) ppb and 59(4) ppb, respectively. In the core of the plume maximum concentrations of particles, CO, and O₃ were observed, where the gas concentrations reached 183 and 75 ppb, respectively. The increased concentration of these trace gases in the plume is consistent with results from other plumes associated with the burning of biomass (Forster et al., 2001; Fiebig et al., 2003; Real et al., 2007). Furthermore, our measurements of enhanced O₃ concentrations and increased temperatures in the plume agree with these previous observations.

It proved difficult, however, to determine the source region of the plume. Using the air mass transport model FLEXPART (e.g. Stohl et al., 2005) we investigated the origin of the air during different parts of the flight. Unfortunately, the analysis rendered inconclusive as the model suggested both contributions from North America as well as Russia. The fact that the model did not pick up the plume can probably be explained by the imperfection in emission fields and the numerics in the model. Especially if the source is intermittent, such as forest fires, it is possible for the model to miss these plumes simply because the source not accurately portrayed in the emission field.

Satellite-images from both MODIS and CALIPSO/CloudSat have been studied for the time and location of interest. It is a complicated analysis to perform as one has to locate the time and area in which the plume is located, which has been difficult as the transport model shows a disperse transport for the time

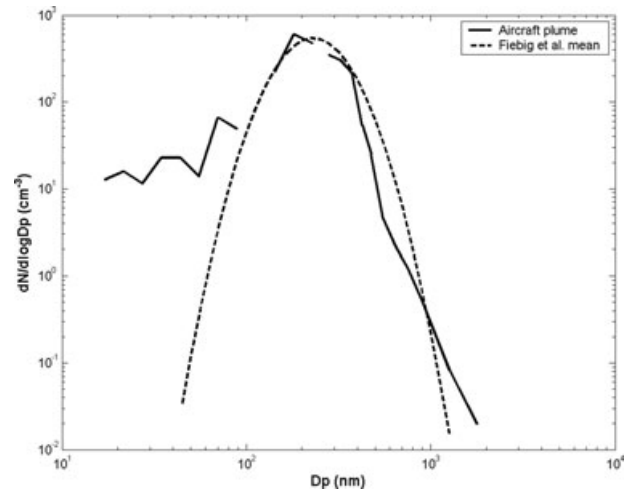


Fig. 3. The measured size distribution within the plume from the aircraft during ASTAR2007 (solid line) compared to the size distribution observed over Europe (dashed line) by Fiebig et al. (2003)

period of interest. Furthermore, the plume appears to be narrow both horizontally and vertically, which results in difficulties to trace it on satellite images. However, plumes like these, even though they are 'subvisible', are believed to have a significant effect on the radiation budget due to the conditions in the Arctic, especially high-surface albedo. As shown below, the aerosol characteristics are very similar to previously published biomass plume properties and we will concentrate on the effects of such aerosol layers in the Arctic free atmosphere without drawing any conclusions from analyses regarding the source region.

In the contaminated layer the maximum particle concentration for N₂₆₀ detected by the OPC was 207 cm⁻³, with a size-distribution mode around 270 nm, whereas the N₁₀ does not show a corresponding number-density increase. The N₂₆₀ concentration in the FT was around one order of magnitude smaller, with mean and standard deviation concentrations of 20 (7) cm⁻³ and the mode of the particles centred between 150 and 190 nm. These aerosol size distributions are very similar to those expected from biomass burning; the observed size distribution furthermore shows many similarities (cf. Fig. 3) with that of a forest-fire plume (Fiebig et al., 2003) which originated in Canada and was detected over continental Europe. The heat-treated aerosol size distribution indicates that particles smaller than 60 nm disappear when heat treated, whereas particles larger than 60 nm 75% or more left a residue indicating internally mixed aerosol. (These ratios also hold true outside the plume.)

The accumulation-mode size range indicates that we sampled an aged air-mass, where growth processes due to condensation and coagulation have affected the size distribution and its mixing state. The growth processes in a smoke plume are known to be equally dominated by condensation and coagulation/gas-to-particle conversion during the first 1–4 d, after which time coagulation dominates the ageing process (Reid et al., 1998).

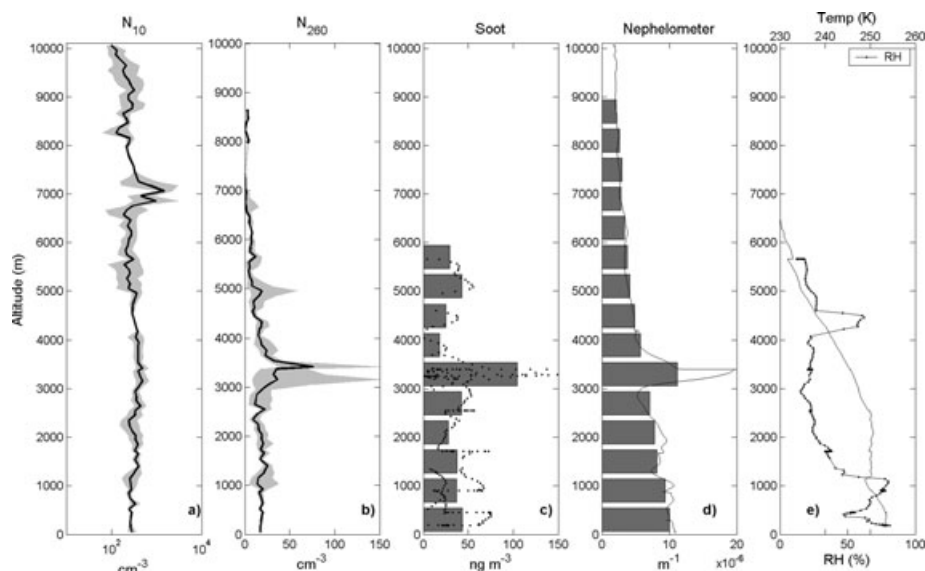


Fig. 4. (a) The number densities for the total number of particles larger than 10 nm (N_{10}) and (b) the total number of particles larger than 260 nm (N_{260}) (c) the estimated soot concentration from the aircraft measurement which is applied in the model (bars) and the corresponding measured values from the aircraft (dots), (d) the corresponding scattering measured with the nephelometer onboard the aircraft, input for the model (bars) and the measured values from the aircraft (line) and (e) temperature (solid line) and relative humidity (RH) (dotted line) measured onboard the aircraft.

The amount of light-absorbing particles is enhanced in the polluted layer; assuming soot to dominate the absorbing fraction, the estimated concentrations are in the range 90–350 ng m^{-3} [whereas the background FT concentration is 36 (16) ng m^{-3}]. The soot concentrations in the Arctic vary considerably over the year, with a polluted spring and clean summer conditions. During the flight on April 14, it was between 50 and 300 ng m^{-3} , compared to a multiyear quartile range between approximately by 20 and 60 ng m^{-3} based on Zeppelin observations in April.

As regards the aircraft-measured scattering coefficients, the profile shows a general decrease from the surface up to the top

flight level near the tropopause (from $10 \times 10^{-6} \text{ m}^{-1}$ at the surface to $2 \times 10^{-6} \text{ m}^{-1}$ at the top), with a maximum value of $20 \times 10^{-6} \text{ m}^{-1}$ in the polluted layer, Fig. 4d.

The meteorological data measured from the aircraft show a stable stratification in the atmosphere. It appears as if, when entering the plume, there is a temperature increase of a few tenths of a degree. The vertical temperature perturbation in the plume can be seen in Fig. 5. The relative humidity in the core of the plume was around 10%, consistent with a diabatic warming of the layer caused by light-absorbing aerosols. It is thus suggested that the soot gives rise to radiative convection or lofting of the plume. During the ASTAR campaign low values of relative humidity have been observed above cloud tops and when stratospheric intrusions take place in the higher troposphere. The relative humidity above and below the plume was found to be up to 90 and 25%, respectively.

4.2. The radiative effects of the haze layer

To examine the local heating of the perturbed layer we calculated the vertical distribution of the heating rate using the one-dimensional radiation model described in Section 3. The input to the model is provided by the previously described observational data set. The data are averaged over 600-m bins from the surface up to 8400 m, (Figs. 4 c and d).

The volatility DMPS observations indicate that the optically active size range of the aerosol size distribution was internally mixed. Thus, our heating rate calculations assume the entire aerosol population to be internally mixed. We make three different calculations based on the minimum (min.), maximum (max.)

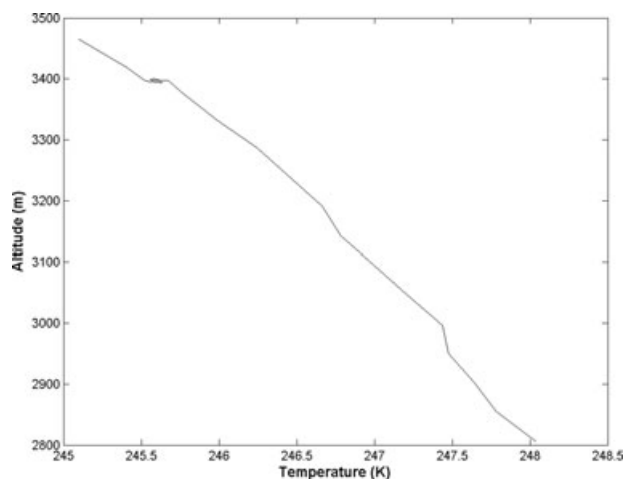


Fig. 5. The measured temperature profile where the plume was detected.

and mean properties in each altitude bin. The calculations using the extreme values are performed in order to achieve a rough estimate of the possible range of values. Heating rates were calculated for two different surface albedos, where 0.9 represents an ice/snow covered surface, and 0.15 represents an open ocean. The main part of the mission flight took place over an ice-covered ocean with a varying fraction of open leads. The summer sea-ice extent has decreased very rapidly over the last years and the open ocean albedo may be a more representative condition for the Arctic summer in the near future.

The resulting profiles, using altitude bins as in Fig. 4, for an albedo of 0.9 and 0.15 are presented in Figs. 6a and b. For

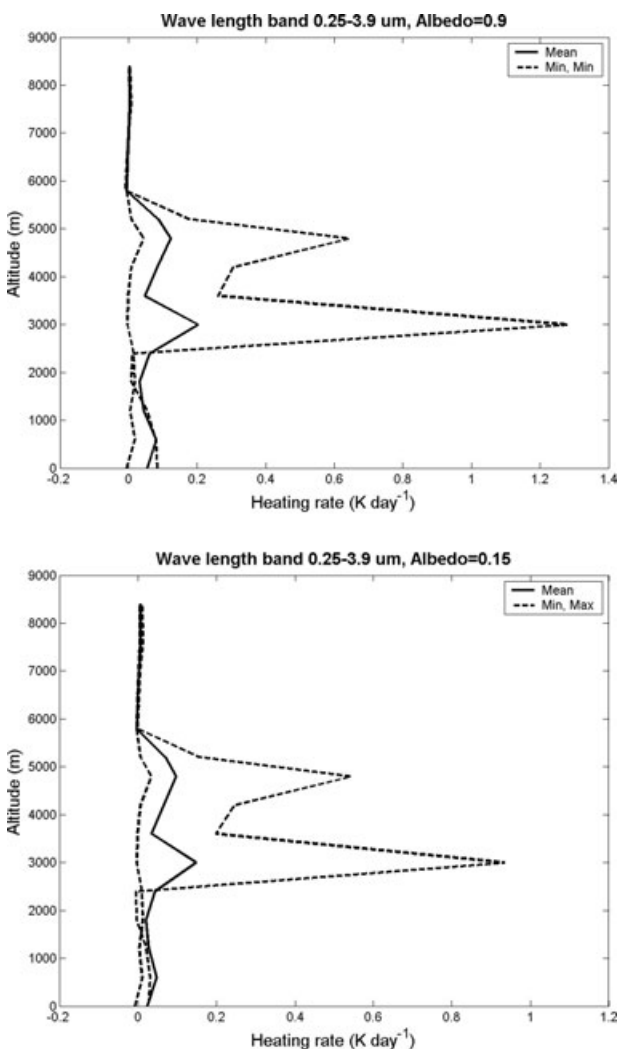


Fig. 6. Top panel: the model calculations of the heating rates for an albedo = 0.9 representing an ice/snow covered ocean. Thick solid line = 'mean condition', thick dashed line = 'extreme condition', thin dashed lines = 'min. and max. condition' of the measured input variables. Bottom panel: the corresponding model calculations for an albedo = 0.15 representing an ice-free ocean.

the high-albedo case, an additional calculation was performed, where average values were used in all bins except for the plume altitude bin between 3000 and 3600 m. For this bin the maximum soot concentration observed over this altitude range was assumed to be valid for the entire bin. This enhances the absorption in the layer while retaining the scattering properties at the average values.

The minimum-condition calculations show very low heating rates, and only a small enhancement can be seen near 5 km altitude. The maximum-condition, on the other hand, presents a heating rate of up to 1.3 K d⁻¹ in the plume layer. The heating rate for the average condition drops significantly to 0.2 K d⁻¹ in the plume layer, and near 5 km it is a little more than 0.1 K d⁻¹. The simulation with average conditions except in the plume layer presents a heating rate between the mean-case and the max-case of 0.6 K d⁻¹. This illustrates the strong impact on the heating rate that a combined enhanced scattering and absorbing aerosol will have despite the relatively dry air.

Reducing the surface albedo brings about a decrease in the heating rates as illustrated in Fig. 6b. The overall reduction is around 25%. In the plume layer, the heating rates are reduced from 0.2 to 0.15 and from 1.3 to 1 K d⁻¹ for the mean-condition and max.-condition, respectively. These results are consistent with those from Ramaswamy et al. (2001), who reported the dependence of radiative effects on the surface albedo and showed how the presence of BC in the atmosphere may give rise to significant positive forcing over highly reflecting surfaces such as clouds or snow/ice.

5. Summary and discussion

In this study, we have shown that transport of pollutants from the mid-latitudes into the Arctic free troposphere may give rise to a heating rate within the plume of up to 1.3 K d⁻¹, dependent on the properties of the plume and the surface albedo. The surface properties, in this study ice/snow covered or ice-free ocean, are of importance since the latter case with a low albedo shows a 25–30% decrease of the heating rate compared to the snow/ice case. These results can be compared to those obtained by Treffeisen et al. (2007), who estimated a heating rate of 1.7 K d⁻¹ at an altitude of 0.5 km based on the observed concentrations of particles, soot, and aerosol scattering during the highest pollution event ever recorded at Svalbard. Our 'mean-case' model results are furthermore consistent with a theoretical analysis inspired by a haze event during ASTAR 2000, in the course of which a heating rate of 0.3 K d⁻¹ at 2 km altitude was calculated (Treffeisen et al., 2005).

Beside the direct radiative effects on the Arctic atmosphere, the aerosol originating from the burning of biomass has an effect on the probability of forming ice clouds during a period of the year when the atmosphere is marginally conditional for spontaneous freezing. This could have effects on the rain out processes (cf. Jensen and Toon, 1997; Diehl et al., 2006), but a

closer examination of these processes lies beyond the focus of the present study on the radiative effects of the aerosol.

Our estimates of the heating rate constrained by observed aerosol characteristics corroborate older literature such as Mitchell (1971) and emphasize the importance of aerosol layers above high-albedo surfaces. In this study, we have shown that upper-layer transport of soot from lower latitudes into the Arctic may be of importance for the radiative budget in the Arctic troposphere. The overall impact of these events, however, is difficult to quantify due to the high altitudes at which the transport take place.

6. Acknowledgments

The authors thank the pilots and the crew of the Falcon 20 research aircraft and K. Hara at the National Institute of Polar Research, Japan, for providing the nephelometer onboard the Falcon. The authors acknowledge Birgitta Noone and Juri Waher for invaluable help with collecting the data from the Zeppelin station. Acknowledge to the Swedish Research Council and the Swedish Environmental Protection Agency for supporting this study.

References

- Chang, H. and Charalampopoulos, T. T. 1990. Determination of the wavelength dependence of refractive-indexes of flame soot. *Proc. R. Soc. Lond. Ser. A-Math. Phys. Eng. Sci.* **430**, 577–591.
- Diehl, K., Simmel, M. and Wurzler, S. 2006. Numerical sensitivity studies on the impact of aerosol properties and drop freezing modes on the glaciation, microphysics, and dynamics of clouds. *J. Geophys. Res.-Atmos.* **111**, D07202, doi:10.1029/2005JD005884.
- Engvall, A. C., Krejci, R., Ström, J., Minikin, A., Treffeisen, R. and co-authors. 2008. In-situ airborne observations of the microphysical properties of the Arctic tropospheric aerosol during late spring and summer. *Tellus* **60B**, 392–404.
- Fiebig, M., Stohl, A., Wendisch, M., Eckhardt, S. and Petzold, A. 2003. Dependence of solar radiative forcing of forest fire aerosol on ageing and state of mixture. *Atmos. Chem. Phys.* **3**, 881–891.
- Forster, C., Wandering, U., Wotawa, G., James, P., Mattis, I. and co-authors. 2001. Transport of boreal forest fire emissions from Canada to Europe. *J. Geophys. Res.-Atmos.* **106**, 22887–22906.
- Hansen, J. and Nazarenko, L. 2004. Soot climate forcing via snow and ice albedos. *Proc. Natl. Acad. Sci. U.S.A.* **101**, 423–428.
- Huntrieser, H., Schlager, H., Roiger, A., Lichtenstern, M., Schumann, U. and co-authors. 2007. Lightning-produced NO_x over Brazil during TROCCINOX: airborne measurements in tropical and subtropical thunderstorms and the importance of mesoscale convective systems. *Atmos. Chem. Phys.* **7**, 2987–3013.
- IPCC. 2007. Contribution of Working Group I to the Fourth Assessment Report of the Intergovernmental Panel on Climate Change. In: *Climate Change 2007: The Physical Science Basis* (eds S. Solomon, D. Qin, M. Manning, Z. Chen, M. Marquis, K. B. Averyt, M. Tignor and H. L. Miller). Summary for Policymakers. Cambridge University Press, Cambridge, United Kingdom and New York, NY, USA, 1–18.
- Jacobson, M. Z. 2001. Strong radiative heating due to the mixing state of black carbon in atmospheric aerosols. *Nature* **409**, 695–697.
- Jensen, E. J. and Toon, O. B. 1997. The potential impact of soot particles from aircraft exhaust on cirrus clouds. *Geophys. Res. Lett.* **24**, 249–252.
- Köpke, P., Hess, H., Schult, I. and Shettle, E. 1997. The Global Aerosol Data Set (GADS). MPI-Rep., Hamburg 243, 44.
- Lavoué, D., Lioussé, C., Cachier, H., Stocks, B. J. and Goldammer, J. G. 2000. Modeling of carbonaceous particles emitted by boreal and temperate wildfires at northern latitudes. *J. Geophys. Res.-Atmos.* **105**, 26871–26890.
- Lohmann, U. and Feichter, J. 2005. Global indirect aerosol effects: a review. *Atmos. Chem. Phys.* **5**, 715–737.
- Mitchell, J. M. 1971. The effect of atmospheric aerosols on climate with special reference to temperature near the Earth's surface. *J. Appl. Meteor.* **10**, 703–714.
- Penner, J. E., Chuang, C. C. and Grant, K. 1998. Climate forcing by carbonaceous and sulfate aerosols. *Clim. Dyn.* **14**, 839–851.
- Petzold, A., Kopp, C. and Niessner, R. 1997. The dependence of the specific attenuation cross-section on black carbon mass fraction and particle size. *Atmos. Environ.* **31**, 661–672.
- Quinn, P. K., Bates, T. S., Baum, E., Doubleday, N., Fiore, A. M. and co-authors. 2008. Short-lived pollutants in the Arctic: their climate impact and possible mitigation strategies. *Atmos. Chem. Phys.* **8**, 1723–1735.
- Ramaswamy, V., Boucher, O., Haigh, D., Hauglustaine, J., Haywood, J. M. and co-authors. 2001. Radiative forcing of climate change. In: *Climate Change 2001: The Scientific Basis*. (eds J. T. Houghton and co-editors.) Contribution of Working Group I to the Third Assessment Report of the Intergovernmental Panel on Climate Change. Cambridge University Press, Cambridge, United Kingdom and New York, NY, USA, 349–416.
- Real, E., Law, K. S., Weinzierl, B., Fiebig, M., Petzold, A. and co-authors. 2007. Processes influencing ozone levels in Alaskan forest fire plumes during long-range transport over the North Atlantic. *J. Geophys. Res.-Atmos.* **112**, D10S41, doi:10.1029/2006JD007576.
- Reid, J. S., Hobbs, P. V., Ferek, R. J., Blake, D., Martins, J. V. and co-authors. 1998. Physical, chemical, and optical properties of regional hazes dominated by smoke in Brazil. *J. Geophys. Res.-Atmos.* **103**, 32059–32080.
- Ricchiazzi, P., Yang, S. R., Gautier, C. and Sowle, D. 1998. SBDART: a research and teaching software tool for plane-parallel radiative transfer in the Earth's atmosphere. *Bull. Am. Meteorol. Soc.* **79**, 2101–2114.
- Rinke, A., Dethloff, K. and Fortmann, M. 2004. Regional climate effects of Arctic Haze. *Geophys. Res. Lett.* **31**, L16202, doi:10.1029/2004GL020318.
- Schröder, F. and Ström, J. 1997. Aircraft measurements of sub micrometer aerosol particles (>7 nm) in the midlatitude free troposphere and tropopause region. *Atmos. Res.* **44**, 333–356.
- Seinfeld, J. 2008. Black carbon and brown clouds. *Nat. Geosci.* **1**, 15–16.
- Stohl, A., Forster, C., Frank, A., Seibert, P. and Wotawa, G. 2005. Technical note: the Lagrangian particle dispersion model FLEXPART version 6.2. *Atmos. Chem. Phys.* **5**, 2461–2474.
- Stohl, A., Andrews, E., Burkhardt, J. F., Forster, C., Herber, A. and co-authors. 2006. Pan-Arctic enhancements of light absorbing aerosol concentrations due to North American boreal forest fires during summer 2004. *J. Geophys. Res.-Atmos.* **111**, D22214, doi:10.1029/2006JD007216.

- Ström, J., Umegård, J., Tørseth, K., Tunved, P., Hansson, H. C. and co-authors. 2003. One year of particle size distribution and aerosol chemical composition measurements at the Zeppelin Station, Svalbard, March 2000–March 2001. *Phys. Chem. Earth* **28**, 1181–1190.
- Treffeisen, R., Herber, A., Ström, J., Shiobara, M., Yamanouchi, T. and co-authors. 2004. Interpretation of Arctic aerosol properties using cluster analysis applied to observations in the Svalbard area. *Tellus* **56B**, 457–476.
- Treffeisen, R., Rinke, A., Fortmann, M., Dethloff, K., Herber, A. and co-authors. 2005. A case study of the radiative effects of Arctic aerosols in March 2000. *Atmos. Environ.* **39**, 899–911.
- Treffeisen, R., Tunved, P., Ström, J., Herber, A., Bareiss, J. and co-authors. 2007. Arctic smoke— aerosol characteristics during a record smoke event in the European Arctic and its radiative impact. *Atmos. Chem. Phys.* **7**, 3035–3053.
- Wiscombe, W. 1979. Mie scattering calculations: advances in technique and fast, vector-speed computer codes. NCAR Technical Note NCAR/TN-140+STR, available from National Technical Information Service as NTIS PB 301388.